Controlled source interferometry with noisy data

Jürg Hunziker, Joost van der Neut, Evert Slob and Kees Wapenaar, Delft University of Technology*

SUMMARY

We investigate the effects of noise on controlled-source interferometry by multi-dimensional deconvolution (MDD) for diffusive electromagnetic (EM) fields and for seismic wavefields. An electromagnetic and a seismic dataset are modeled and decomposed into up- and downwards decaying and up- and downgoing fields, respectively. From the decomposed fields a reflection response can be retrieved using least-squares inversion. We show, that noise affects the EM data differently than seismic data due to the diffusive nature of the EM fields.

INTRODUCTION

In seismics, interferometry is well known as the process of cross-correlating two traces at two receiver positions to retrieve the Green's function between these two receivers. The theory has been derived and applied for controlled-source and passive cases by various authors. Wapenaar et al. (2008a) and Schuster (2009) give a comprehensive overview. Interferometry by cross-correlation has also been derived for electromagnetics (Slob et al., 2007).

Cross-correlation can be replaced by a multi-dimensional deconvolution (MDD) in the controlled-source case (Wapenaar et al., 2008b) and in the passive case (Wapenaar et al., 2008c). Interferometry by MDD consists mainly of two steps. First the fields need to be decomposed into up- and downgoing fields and then a reflection response is retrieved from the separated fields as if there would be sources, radiating downwards, at the receiver positions. This reflection response contains only reflections from below the receivers. This means that with MDD, structures above the receivers are simply replaced by a halfspace with the same parameters as the subsurface right below the receivers, thus eliminating all primaries and multiples from above.

In this paper we investigate the effect of noisy data for controlled-source electromagnetic (EM) and seismic interferometry by MDD. Special focus is given on the illumination matrix, i.e. the matrix which needs to be inverted in the MDD process, and how uncorrelated noise affects the inversion process.

THEORY

The electromagnetic fields are decomposed into flux normalized up- and downwards decaying fields using an algorithm derived by Slob (2009). Similarly the seismic wavefields are decomposed into flux normalized up- and downgoing fields (Wapenaar et al., 2008b). In both cases the up- and downgoing fields are represented with $\hat{P}^-(\mathbf{x_R},\mathbf{x_S})$ and $\hat{P}^+(\mathbf{x_R},\mathbf{x_S})$ respectively. The circumflex denotes space-frequency domain, but for simplicity the frequency dependence of all variables is omitted. The receiver coordinates are represented by $\mathbf{x_R}$ and the source coordinates by $\mathbf{x_S}$. The decomposition can be done at any depth level where no sources are present. The implementation used here assumes the material parameters to be laterally constant at the depth level of decomposition. The decomposed fields are related to each other through the reflection response $\hat{R}_0^+(\mathbf{x_R},\mathbf{x'_R})$:

$$\hat{P}^-(\mathbf{x_R},\mathbf{x_S}) = \int_{\partial D_R} \hat{R}_0^+(\mathbf{x_R},\mathbf{x'_R})\hat{P}^+(\mathbf{x'_R},\mathbf{x_S})dx'_R, \qquad (1)$$

where the integration is taken over all receivers. The superscript $^+$ in the reflection response indicates that its origin is a downgoing field and the subscript $_0$ represents the absence of heterogeneities above the receiver level. This equation can be rewritten in matrix notation (Berkhout, 1982) as

$$\hat{\mathbf{P}}^- = \hat{\mathbf{R}}_0^+\hat{\mathbf{P}}^+. \qquad (2)$$

Each column of the matrices contains various receiver positions but a fixed source position and vice versa for the rows. Interferometry by MDD solves equation 2 for $\hat{\mathbf{R}}_0^+$ with a least-squares inversion:

$$\hat{\mathbf{R}}_\mathbf{0}^+ = \hat{\mathbf{P}}^- \left(\hat{\mathbf{P}}^+\right)^\dagger \left[\hat{\mathbf{P}}^+ \left(\hat{\mathbf{P}}^+\right)^\dagger + \varepsilon^2\mathbf{I}\right]^{-1}. \qquad (3)$$

The superscript † denotes complex-conjugation and transposition and $\mathbf{I}$ is the identity matrix. The stabilization parameter ε prevents the inversion from getting unstable.

To investigate noise effects, uncorrelated noise is added to the data before decomposition. Since the inversion can be an unstable process, the effects of the noise on the inversion are of special interest. Therefore we rewrite the illumination matrix $\hat{\mathbf{P}}^+(\hat{\mathbf{P}}^+)^\dagger$, the matrix which needs to be inverted, as follows:

$$\begin{aligned}\hat{\mathbf{P}}^+ \left(\hat{\mathbf{P}}^+\right)^\dagger &= \left(\hat{\mathbf{P}}_c^+ + \hat{\mathbf{N}}^+\right)\left(\hat{\mathbf{P}}_c^+ + \hat{\mathbf{N}}^+\right)^\dagger \\ &= \hat{\mathbf{P}}_c^+ \left(\hat{\mathbf{P}}_c^+\right)^\dagger + \hat{\mathbf{P}}_c^+ \left(\hat{\mathbf{N}}^+\right)^\dagger + \\ &\quad \hat{\mathbf{N}}^+ \left(\hat{\mathbf{P}}_c^+\right)^\dagger + \hat{\mathbf{N}}^+ \left(\hat{\mathbf{N}}^+\right)^\dagger, \qquad (4)\end{aligned}$$

where $\hat{\mathbf{N}}^+$ is the noise found in the downgoing fields and the subscript $_c$ stands for clean and means that the data is free of noise. In the following sections the different terms of equation 4 are analyzed.

MODELING AND PROCESSING

A synthetic EM dataset with a J_x source towed behind a boat and 512 E_x and H_x receivers at the ocean bottom (2D TM setup) is modeled in the wavenumber domain, where J represents an electric source whose antenna orientation is given by the subscript. The source emits at 1024 different positions

a signal at 0.5 Hz. The electric and magnetic field components are represented by E and H respectively. Their receiver component is also indicated by the subscript. The source and the receiver spacings are 80 m. The dataset consists from top to bottom of a halfspace of air, a water layer and halfspace of ground. The latter is intersected by a reservoir layer. All electric and geometrical parameters of the model are given in Figure 1.

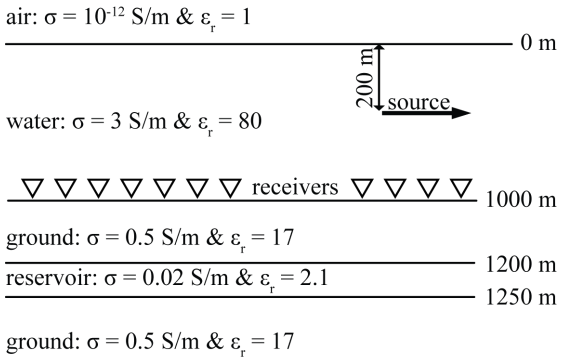

Figure 1: Setup of electromagnetic modeling: The black arrow indicates the source, white triangles the receivers. Conductivity σ and relative permittivity ε_r are given in the layers.

A second, in this case elastic seismic dataset, is modeled with 501 sources at the surface and 101 receivers in a horizontal borehole at a depth of 800 m. The source spacing is 8 m and the receiver spacing 16 m. Here we focus on P-waves only. The layered earth velocity model is shown in Figure 2.

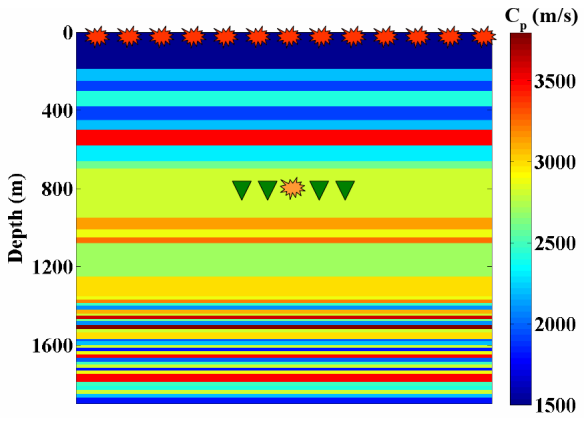

Figure 2: Setup of elastic modeling: The velocities are given in m/s. The red explosion symbols stand for the active sources at the surface, the green triangles for the receivers in the borehole. The orange explosion symbol represents a retrieved source at a receiver position.

After modeling, uncorrelated noise is added to the data in the space domain. Subsequently both datasets are Fourier transformed to the wavenumber domain, where they are decomposed in up- and downwards decaying fields (EM) and up- and downgoing wavefields (seismic). After an inverse Fourier transformation back to space domain, the terms of equation 4 are analysed. For this, also a dataset without noise is decomposed forming $\hat{\mathbf{P}}_c^+$. The noise term $\hat{\mathbf{N}}^+$ can be extracted by subtracting a clean decomposed dataset from a decomposed dataset with noise. Finally equation 3 is solved to retrieve $\hat{\mathbf{R}}_{\mathbf{0}}^+$.

RESULTS

In Figure 3 a) the illumination matrix $\hat{\mathbf{P}}^+(\hat{\mathbf{P}}^+)^\dagger$ is shown for the noise-free EM dataset. To solve equation 3 this matrix needs to be inverted. Because of the laterally invariant setup of the dataset, the illumination matrix features a perfect Toeplitz structure with high amplitudes around the diagonal and low amplitudes at the off-diagonal elements. The different terms according to equation 4 are shown for one line on a logarithmic scale for different noise levels in the EM case in Figure 3 b), c) and d). In red the actual signal $\hat{\mathbf{P}}_c^+(\hat{\mathbf{P}}_c^+)^\dagger$ without noise is plotted. The green curve shows the correlation of the signal with the noise $\hat{\mathbf{P}}_c^+(\hat{\mathbf{N}}^+)^\dagger + \hat{\mathbf{N}}^+(\hat{\mathbf{P}}_c^+)^\dagger$. At last the blue curve representing the autocorrelation of the noise $\hat{\mathbf{N}}^+(\hat{\mathbf{N}}^+)^\dagger$ can be seen. The last one features a clear peak in the center. With increasing noiselevel, the terms containing noise grow in amplitude and would finally cover the signal (not shown). The autocorrelation of the noise (blue curve) never exceeds the amplitude of the correlation of the signal with the noise (green curve).

The illumination matrix for the seismic case is plotted in Figure 4 a) at a frequency of 20 Hz. Again a perfect Toeplitz structure is visible, but this time, the off-diagonal elements have similar amplitudes as the elements on the diagonal. As in the EM case, the different terms of equation 4 are shown for one line of the illumination matrix in Figure 4 b), c) and d). Note that for the seismic case, the scale is linear, whereas it is logarithmic for the EM case. As in the EM case, a clear peak in the autocorrelation term of the noise (blue curve) is visible. In contrast to EM, this peak rises above the curve showing the correlation of the signal with the noise (green curve) and mainly the peak gets larger in amplitude with increasing noise for seismics. This peak in the autocorrelation of the noise supports the stabilization of the inversion in the same way as the actual stabilization parameter ε in equation 3 does.

Finally, the reflection response is retrieved by solving equation 3. Figures 5 and 6 show the retrieved reflection response (red) and the directly modeled reflection response (black) in comparison for the EM and the seismic case, respectively. The noiselevel in the EM case is 10^{-10} and in the seismic case the noise to signal ratio is 0.75. In the EM case, the noise causes minor amplitude errors in the retrieved reflection response at the peak at zero offset and at the peaks at offsets of around 1000 m. More pronounced are the artifacts found at the large offsets, were the retrieved reflection response increases in amplitude, whereas the directly modeled reflection response continues to decay slightly. In seismics, the noise causes small amplitude disturbances best visible at early times. The large reflection between 0.5 and 0.6 s is barely affected by the noise. Reflections at later times suffer also slightly from amplitude disturbances caused by the noise.

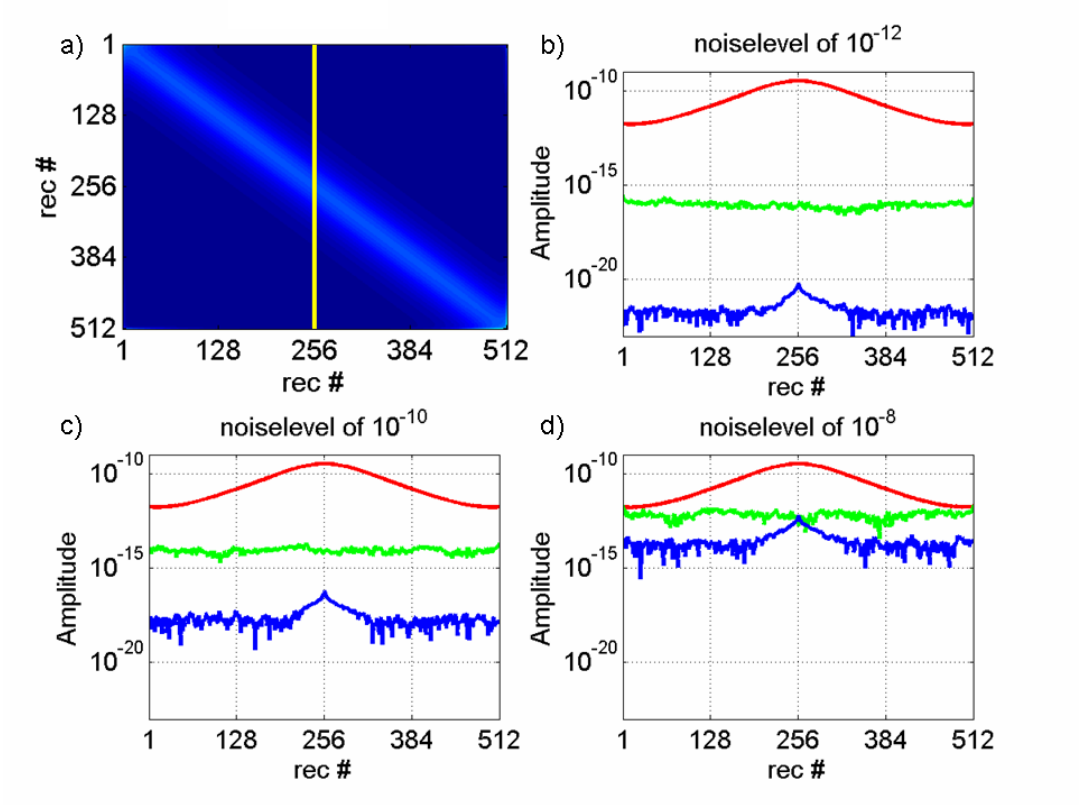

Figure 3: a) Illumination matrix $\hat{\mathbf{P}}^{+}(\hat{\mathbf{P}}^{+})^{\dagger}$ for the noise-free EM case. b) to d) One slice of the matrix $\hat{\mathbf{P}}^{+}(\hat{\mathbf{P}}^{+})^{\dagger}$ for the EM case on a logarithmic scale. This specific slice is indicated with a yellow line in a). The illumination matrix is split up in the different terms $\hat{\mathbf{P}}_c^{+}(\hat{\mathbf{P}}_c^{+})^{\dagger}$ (red), $\hat{\mathbf{P}}_c^{+}(\hat{\mathbf{N}}^{+})^{\dagger}+\hat{\mathbf{N}}^{+}(\hat{\mathbf{P}}_c^{+})^{\dagger}$ (green) and $\hat{\mathbf{N}}^{+}(\hat{\mathbf{N}}^{+})^{\dagger}$ (blue) for different levels of noise. b) noiselevel of 10^{-12}, c) noiselevel of 10^{-10}, d) noiselevel of 10^{-8}.

DISCUSSION

In seismics the autocorrelation of the uncorrelated noise contributes to the diagonal elements of the illumination matrix and the terms containing the correlation of the signal with the noise remains comparably small, but in the EM case the autocorrelation of the noise is much smaller than the terms containing the correlation of the noise with the signal. The reason for this difference lies in the diffusive nature of the EM fields. The Green's function in a fullspace in the space domain is:

$$G = \frac{e^{-ikR}}{4\pi R}, \tag{5}$$

where R is the distance from the source position. The parameter k is for the seismic case $\sqrt{\omega^2/c^2}$ with ω being the angular frequency and c the wave speed. In the EM case k becomes the complex expression $\sqrt{\omega^2/c^2 - i\omega\mu\sigma}$ with the imaginary unit i, the magnetic permeability μ and the conductivity σ. Since the first term, which is the same expression as in seismics, is rather small in EM, k is approximated $\sqrt{-i\omega\mu\sigma}$. This second term adds a large exponential decay causing the EM fields to decay eventually faster. Consequently the illumination matrix for the EM case (Figure 3a) contains much smaller off-diagonal elements compared to the elements on the diagonal than in the illumination matrix for the seismic case (Figure 4b). Therefore in seismics, the terms containing the crosscorrelation of the signal with the noise $\hat{\mathbf{P}}_c^{+}(\hat{\mathbf{N}}^{+})^{\dagger}+\hat{\mathbf{N}}^{+}(\hat{\mathbf{P}}_c^{+})^{\dagger}$ are averaged out. This process does not take place in the EM case and thus the crosscorrelation of the signal with the noise remains in the data with a high amplitude.

CONCLUSIONS

The effects of noise on controlled-source interferometry by MDD for diffusive EM fields and for seismic wavefields are investigated. High noiselevels disturb the data more in EM, than in seismics, because of the diffusive nature of the EM fields. Still it can be said, that also EM interferometry by MDD can be carried out with realistic levels of noise, which have for a frequency of 0.5 Hz an amplitude between 10^{-7} and 10^{-9} V/m (Constable, 2006; Constable et al., 2008).

ACKNOWLEDGMENTS

This research is supported by the Dutch Technology Foundation STW, applied science division of NWO and the Technology Program of the Ministry of Economic Affairs (grant DCB.7913).

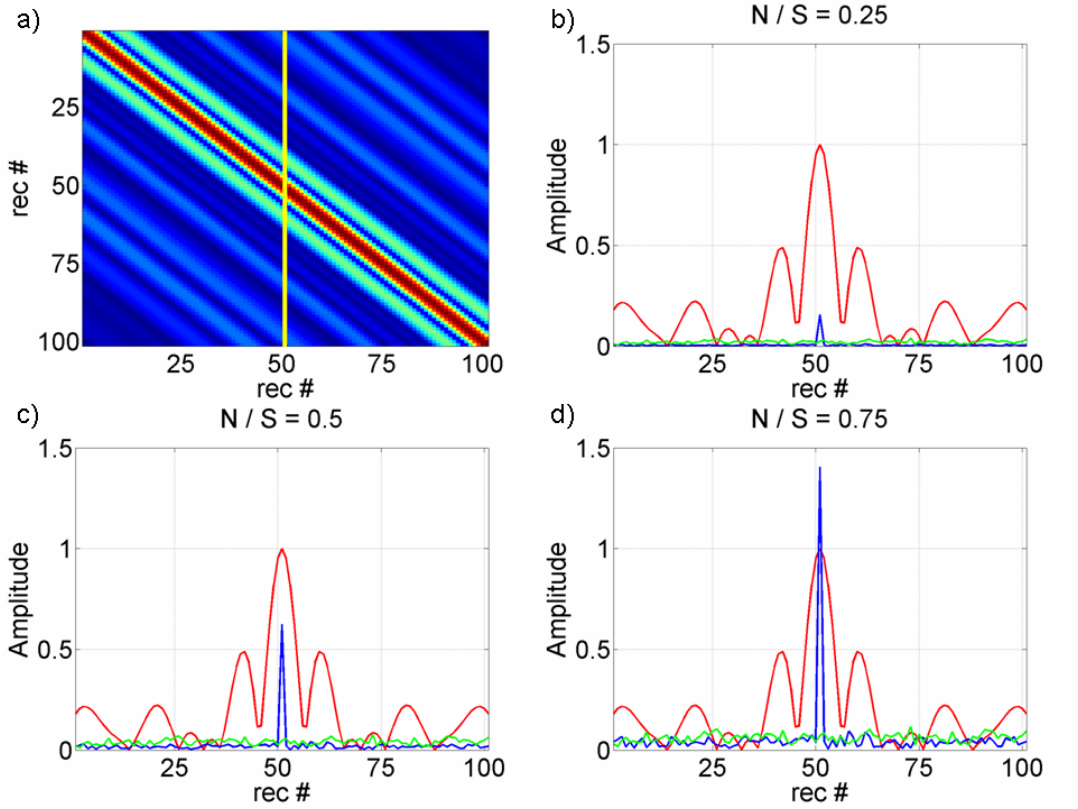

Figure 4: a) Illumination matrix $\hat{\mathbf{P}}^{+}(\hat{\mathbf{P}}^{+})^{\dagger}$ for the noise-free seismic case at 20 Hz. b) to d) One slice of the matrix $\hat{\mathbf{P}}^{+}(\hat{\mathbf{P}}^{+})^{\dagger}$ for the seismic case on a linear scale. This specific slice is indicated with a yellow line in a). The illumination matrix is split up in the different terms $\hat{\mathbf{P}}_c^{+}(\hat{\mathbf{P}}_c^{+})^{\dagger}$ (red), $\hat{\mathbf{P}}_c^{+}(\hat{\mathbf{N}}^{+})^{\dagger}+\hat{\mathbf{N}}^{+}(\hat{\mathbf{P}}_c^{+})^{\dagger}$ (green) and $\hat{\mathbf{N}}^{+}(\hat{\mathbf{N}}^{+})^{\dagger}$ (blue) for different noise to signal ratios. b) N/S = 0.25, c) N/S = 0.5, d) N/S = 0.75.

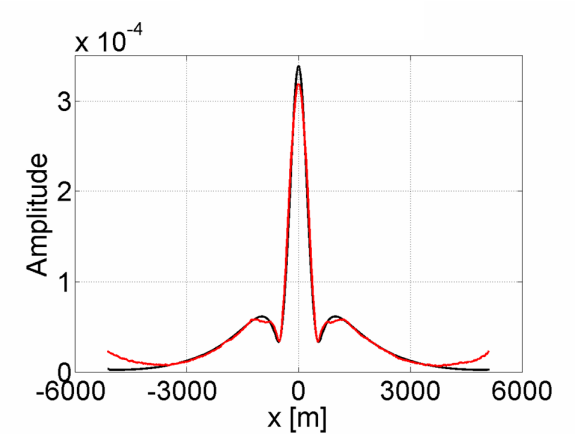

Figure 5: Retrieved reflection response (red) and directly modeled reflection response (black) for the EM case with a noise-level of 10^{-10}.

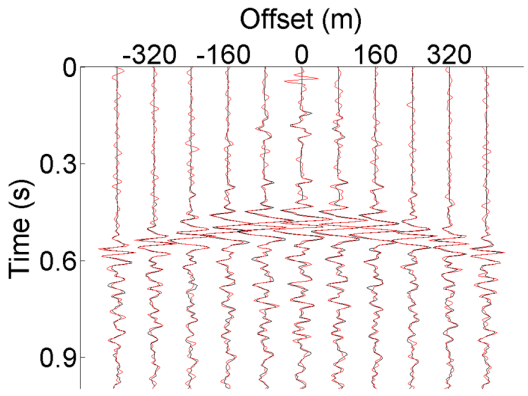

Figure 6: Retrieved reflection response (red) and directly modeled reflection response (black) for the seismic case with a noise to signal ratio of 0.75. (Only 11 of 101 traces are shown.)

REFERENCES

Berkhout, A. J., 1982, Seismic migration. imaging of acoustic energy by wave field extrapolation: Elsevier.

Constable, S. C., 2006, Marine electromagnetic methods - a new tool for offshore exploration: The Leading Edge.

Constable, S. C., A. S. Orange, G. M. Hoversten, and H. F. Morrison, 2008, Marine magnetotellurics for petroleum exploration - part I: A sea-floor equipment system: Geophysics, **63**, 816–825.

Schuster, G., 2009, Seismic interferometry: Cambridge University Press.

Slob, E., 2009, Interferometry by deconvolution of multicomponent multioffset gpr data: IEEE Transactions on Geoscience and Remote Sensing, **47**, 828–838.

Slob, E., D. Draganov, and K. Wapenaar, 2007, Interferometric electromagnetic green's functions representations using propagation invariants: Geophysical Journal International, **169**, 60–80.

Wapenaar, K., D. Draganov, and J. O. A. Robertsson, 2008a, Seismic interferometry: history and present status: Society of Exploration Geophysicists.

Wapenaar, K., E. Slob, and R. Snieder, 2008b, Seismic and electromagnetic controlled-source interferometry in dissipative media: Geophysical Prospecting, **56**, 419–434.

Wapenaar, K., J. van der Neut, and E. Ruigrok, 2008c, Passive seismic interferometry by multidimensional deconvolution: Geophysics, **73**, A51–A56.